"Calculation of Electron Concentration for a Blunt Body at Orbital Speeds and Comparison with Experimental Data," TN D-6294, May 1971, NASA.

[21] Webb, H., Jr. et al., "Theoretical Flow Field Calculations for Project RAM," CR-1308, May 1969, NASA.

[22] DeBolt, H. E. and Port, W., "Thermochemical Equilibrium Studies of Ablative Heat-Shield Materials," RAD-TM-63-27, June 1963, Avco Corp., Research and Advanced Development Div., Wilmington, Mass.

[23] Starner, K. E., "Evaluation of Electron Quench Additives in a Subsonic Air Arc Channel," *AIAA Journal*, Vol. 7, No. 12, Dec. 1969, pp. 2357-2358.

JUNE 1971 AIAA JOURNAL VOL. 9, NO. 6

Effects of Electrode Size on the Performance of a Combustion-Driven MHD Generator

E. S. Rubin* and R. H. Eustis†
Stanford University, Stanford, Calif.

Experiments have been conducted to investigate the effects of electrode size on the performance of a combustion-driven MHD generator. Electrode sizes with length-to-pitch ratios of 0.23, 0.50, and 0.79 were tested in a generator section simulated by three molybdenum electrode pairs located at the downstream end of an MHD channel. Voltage probe data were obtained for electrode surface temperatures between 500°K and 1600°K, with gas conductivity in the electrode boundary-layer regions established independently by either a hot (2200°K MgO brick) or cold (750°K water-cooled plate) upstream wall. At a given load current, larger electrodes were found to have lower voltage losses for similar conditions of surface and gas boundary-layer temperature. For dissimilar boundary layers, reflecting coupling between electrode and boundary-layer temperatures in a cold-electrode generator, total voltage losses for a large electrode pair were equal to or greater than those of a small electrode pair at the same surface temperature. Experimental boundary-layer resistances at anodes were in good agreement with analytical predictions based on both an approximate and a more exact gasdynamic model, for electrode temperatures above about 800°K. At lower temperatures anodes were believed to be influenced by solidification of seed compounds on the electrode surfaces, resulting in higher losses. For cathodes, the boundary-layer resistance was gasdynamic for the case of a hot upstream wall, for electrode current densities below that of saturated thermionic emission at the electrode temperature. In all other cases, the presence of cathode surface-sheath effects was indicated.

I. Introduction

SEGMENTED electrodes have long been used in MHD generators to suppress the internal flow of axial currents (associated with the Hall effect) and thereby improve performance relative to the case of a continuous electrode generator. In the one-dimensional idealization of a generator with infinitely fine electrode segmentation, performance is independent of the Hall parameter for typical MHD conditions.[1] In general, however, real segmented generators are at best two-dimensional and the influence of the Hall effect in the presence of finite electrode sizes cannot be ignored.

Besides altering performance because of the Hall effect, finite-length electrodes may also affect MHD generators by influencing the boundary layers which develop along the electrode walls. Boundary layers that are low in temperatures will have a characteristically low electrical conductivity, which may substantially increase the generator's internal resistance.[2] The boundary-layer temperature, however, is coupled to the electrode temperature, and the degree of coupling is dependent on the ratio of electrode length-to-pitch. Thus, for example, one may expect that the characteristic temperature of a boundary layer developing over an electrode wall of small electrodes and large uncooled insulators will remain relatively insensitive to changes in electrode temperature as compared to the case of large electrodes and small insulators, where strong coupling of electrode and boundary-layer temperatures would be expected. Indeed, the presence of such coupling may negate gains in generator performance anticipated on the basis of a fixed conductivity profile. Additionally, electrode size may have an influence on other phenomena typically encountered in MHD generators, such as arc spots and electrode surface-sheath effects. Such phenomena are not well understood and the effects of electrode size in their presence requires study.

Theoretical treatments of the effects of a finite electrode size on MHD generator performance are fairly extensive in the literature for the case of a channel with uniform electrical conductivity.[3-5] Celinsky and Fischer,[5] for example, showed that variation of the electrode length-to-pitch ratio changed the internal resistance by 50% or more (other conditions fixed), and that an optimum electrode size existed which depended on the channel geometry and on the Hall parameter. More recently, MacDonald, Mitchner, and Oliver[6] have

Received June 12, 1970; revision received January 25, 1971. This work was supported by the Air Force Aero Propulsion Laboratory, Wright-Patterson Air Force Base, Ohio. The authors happily acknowledge the many useful conversations with M. Mitchner, C. H. Kruger, and J. F. Louis, and the help of F. L. Levy of the Stanford Plasma Gasdynamic Laboratory.

* Research Assistant, Mechanical Engineering Department; now Assistant Professor, Mechanical Engineering Department, Carnegie-Mellon University, Pittsburgh, Pa. Associate Member AIAA.

† Professor, Mechanical Engineering Department. Associate Fellow AIAA.

calculated electrode size effects for a nonuniform electrical conductivity profile in which conductivity remained constant through the channel core, but varied linearly through the boundary layers. For a high-conductivity layer near the wall, the optimum electrode size was smaller than for either the low-conductivity or uniform conductivity cases. With low-conductivity layers, resistance increased rapidly with decreasing electrode size, and a larger electrode became preferable in all cases. These latter results of Ref. 6 most closely reflect the effects of electrode size variations expected for the real combustion-gas generators of present interest. The theory, however, is restricted to a gasdynamic loss mechanism, and to conductivity profiles which are only qualitatively accurate.

In the experimental literature, combustion-gas generator tests are reported for a wide spectrum of electrode sizes.[7-9] However, no systematic investigation of electrode size effects appear to have been performed, nor can existing results be accurately correlated.

The experiments to be discussed, then, have an essentially twofold objective. The first is to determine the effects of a varying electrode size on generator performance for fixed values of the geometrical and flow parameters, and for a fixed profile of the electrical conductivity in the electrode-wall boundary layers. Secondly, the experiments seek to compare the effects of electrode size on the performance of generators with dissimilar boundary-layer conductivities. This would reflect effects of coupling between electrode and boundary-layer temperatures which may be particularly prominent in a cold-electrode generator.

II. Experimental Design and Construction

The experimental program was conducted in the Stanford University combustion-driven MHD test facility, whose working fluid was the combustion products of a stoichiometric mixture of ethanol and oxygen diluted with nitrogen and seeded with potassium hydroxide. A detailed description of the system can be found in the works of earlier experimenters.[10,11]

In the present work, three experiments were performed with a generator section composed of three electrode pairs located at the downstream end of an MHD test duct 10 cm × 3.1 cm in cross section. The center pair, or "test" electrodes, was taken as representative of a segmented generator, with the two remaining pairs functioning as "guard" electrodes. This configuration was found to eliminate end effects to a high degree of approximation in both theoretical[12] and experimental[10] studies.

The geometry (Fig. 1) permitted the gas boundary-layer temperature at the test electrode location to be conditioned independently of electrode temperature by separately regulating the temperature of a continuous wall upstream of the electrodes. With appropriate combinations of electrode and upstream wall temperatures, good simulation of both the uncoupled problem (fixed conductivity profile with different electrode sizes) and the coupled problem (dissimilar conductivity profiles with different electrode sizes) was obtainable.

Regulation of the upstream wall temperature was accomplished by using either magnesium oxide ceramic (2200°K), or a water-cooled stainless steel plate (750°K) as the upstream wall material. Electrodes were cooled either with water or nitrogen gas to allow operation at surface temperatures between 500°K and 1600°K. Similar temperatures in the several electrodes were obtained by regulating the coolant flow rate in individual cooling circuits. All electrodes were fabricated of molybdenum, and specially coated to resist oxidation at high temperatures. Channel sidewalls were made of magnesium oxide ceramic.

Three electrode sizes were used for the study. Dimensions in the flow direction yielded electrode length-to-pitch ratios of 0.23, 0.50, and 0.79, with the pitch constant at 4 cm. In all

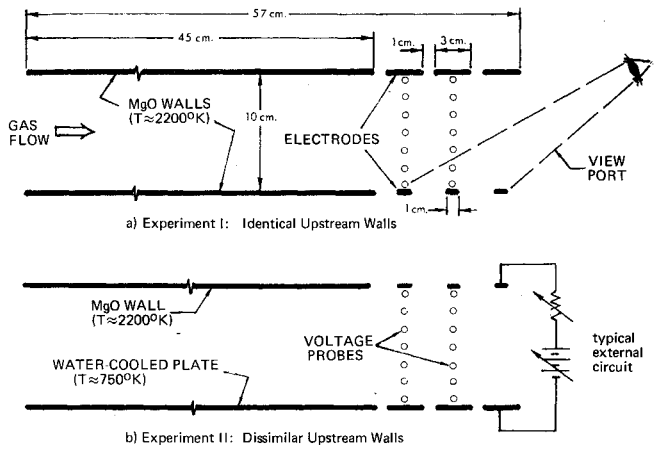

Note: The configuration of Experiment III is similar to Experiment I except for medium (2-cm long) electrodes instead of large electrodes, and with the small electrodes on the upper rather than lower electrode wall.

Fig. 1 Test section configurations for electrode size effect experiments.

experiments two electrode sizes were operated simultaneously (Fig. 1) to assure a comparison of size effects with identical core-gas conditions. Performance was then evaluated in terms of electrode voltage drops determined from sidewall probe measurements. By reversing the polarity of externally applied magnetic and/or electric fields, each electrode size could be operated both as an anode and as a cathode. Prior to conducting experiments in this manner, computer calculations were made to determine whether measurements at either electrode might be influenced by the presence of a different electrode size and conductivity profile at the opposite wall. The study showed that the large, highly conducting gas core typical of the Stanford combustion generator effectively decouples the upper and lower electrode boundary-layer regions, so that electrode voltage drops experienced at one electrode wall are independent of the electrode size and gas conductivity profile at the opposite wall. These results were obtained with a computer program which determines current and potential distributions in MHD generators with nonuniform electrical conductivity, as discussed later in this paper.

In the first of the three experiments the effects of electrode size independent of coupling between electrode and gas boundary-layer temperatures was investigated. Isothermal electrode walls were closely approximated using 1600°K electrodes, and identical MgO walls in the upstream section, as shown schematically in Fig. 1a. This gave essentially the same gas conductivity profile at both the large and small test electrodes. At the same time, the geometry simulated a completely hot-electrode generator for each electrode size. Performance with cold (500°K) electrodes was investigated as well. For all electrode temperatures, variable d.c. power supplied augmented the induced fields by about 30% so as to attain current levels higher than generator short-circuit values.

Experiment II, Fig. 1b, attempted to model the coupled problem for a cold-electrode generator. Here, a continuous cold wall was used upstream of the large electrodes to establish boundary-layer conditions similar to those which might be expected from many additional large cold electrodes in the upstream region. Upstream of the small electrodes a continuous hot wall was retained on the assertion that the temperature of sufficiently small electrodes would have a negligible influence on the boundary-layer temperature profile established by the hot (ceramic) interelectrode insulators. Again, nominal electrode temperatures of 1600°K and 500°K were used, though only the case of cold electrodes was intended to be analogous to a real generator situation for the large electrodes. As before, applied electric fields augmented

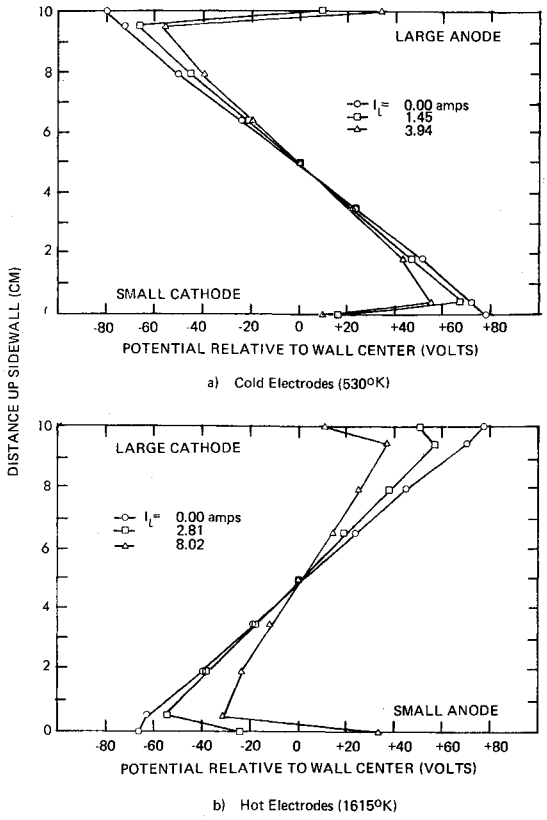

Fig. 2 Transverse potential distributions, identical upstream walls (experiment I).

magnetically induced fields in the uxB direction. Several conditions were repeated without applied power as well.

Experiment III was identical in configuration to experiment I except that the "large" electrodes were replaced by a "medium" electrode size, and the protective electrode coating was removed from the small electrodes to assure it did not influence electrode performance. In this experiment, performance was observed over a carefully defined range of low temperatures to better understand the voltage losses found for cold anodes in experiments I and II. (As discussed later in the paper, these losses were considerably larger than anticipated.) The medium electrode size was also operated at the high temperature of experiment I to obtain additional size-effect data with an isothermal electrode wall.

In each experiment, data were taken only after steady-state operation had been reached at predetermined conditions of mass flow rate, electrode temperature, magnetic field strength, applied voltage, and circuit load resistance. The total duration of each experiment was about $1\frac{1}{2}$ hr. Details of the test procedure, and complete descriptions of instrumentation and data acquisition appear in Ref. 13.

III. Experimental Operating Conditions

Table 1 summarizes pertinent operating conditions for the three experiments. In each case the mass flow rate of combustion gas was 0.271 kg/sec (also, 0.114 kg/sec in experiment III), the seed fraction was 1% potassium by weight, and the mass ratio of nitrogen to oxygen was 0.5. The generator operated in the segmented Faraday mode with a magnetic field strength of 2.65 tesla. Nominal induced electric field in the gas core was 18.5 v/cm.

The thermodynamic state of the test gas was determined locally from the static pressure distribution (measured directly), and the mixed-mean stagnation enthalpy variation (calculated from a system energy balance). The axial distributions of gas velocity and static enthalpy in the core region were then calculated from the continuity and energy equations, taking into account the presence of boundary layers on the four channel walls. Gas temperature, electrical conductivity, and electron mobility (to obtain Hall parameter) then followed from tabulated values of the combustion gas properties. Such values were found to agree well with independent experimental measurements.[13]

The test-electrode surface temperatures indicated in Table 1 represent averages of two temperature measurements per electrode, taken over the time of steady operation. The center and edge temperatures of each electrode were found to be uniform to within 40°K or less, while the temperature of all three electrode pairs were distributed about the mean value with a standard deviation also of about 40°K.

Steady-state surface temperatures of the ceramic upstream wall and interelectrode insulator were found by extrapolating temperatures measured at two depths below the surface, taking into account the temperature dependence of the thermal conductivity of MgO. For the stainless steel upstream wall a single temperature measurement made 0.5 mm below the surface, but corrected for conduction error, was used to obtain the surface temperature. (Conduction error in the electrodes was small due to the higher thermal conductivity of molybdenum.) All upstream wall surface temperatures listed in Table 1 are average values of measurements made at axial locations 17 cm and 1 cm upstream of the electrode section.

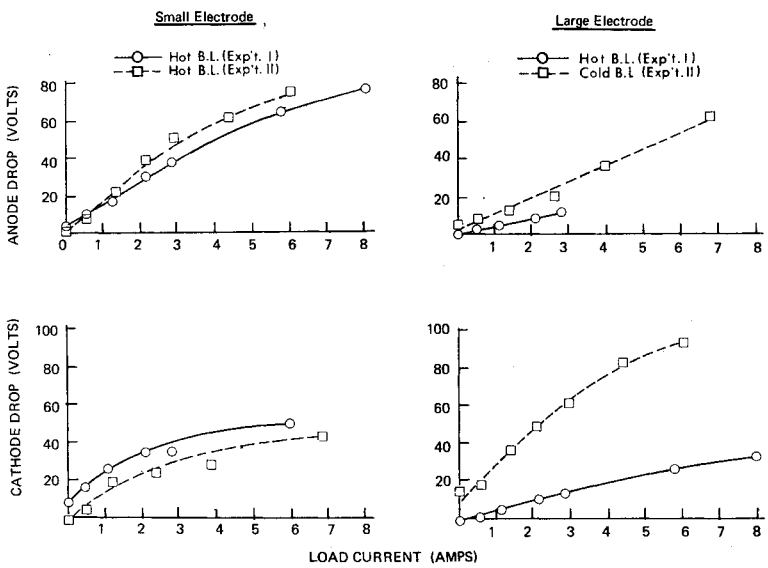

Fig. 3 Comparison of electrode voltage drops, experiments I and II, $T_{electrode}$ = 1615°K.

Table 1 Experimental operating conditions

Case	Core gas properties					Mean surface temperatures, °K		
	Temp., °K	Velocity, m/sec	Press., atm	Conduct., mho/m	Hall no.	Electrodes (cold/hot)	Upstrm Wall (small/lg)	Interelect. (small/lg)
Exp. I	2745	640	1.16	13.0	1.38	530/1615	2310/2285	2230/1625
Exp. II	2715	730	1.05	12.0	1.50	530/1615	2215/750	1920/1550
Exp. III								
a) $\dot{m}$ = 0.27 kg/sec	2720	695	1.05	12.4	1.49	[see Fig. 8]	2300/2380	...
b) $\dot{m}$ = 0.11 kg/sec	2665	300	1.00	9.5	1.53		2210/2165	...

The temperature at these two locations was identical to within about 30°K.

IV. Experimental Results

The basic source of electrical performance data are the electrode voltage drops determined from measurements of probe and electrode potentials to ground. Figure 2 shows several examples of the transverse potential distributions found. For a given current, the electrode voltage drop is defined as the difference between the electrode potential and a potential found by extrapolating the linear voltage profile of the gas core to the electrode wall. Voltage drops thus reflect the combined surface, sheath, and gasdynamic losses of the electrode boundary layer in excess of the potential drop through a boundary layer thickness of core gas.

Hot-Electrode Performance

Anode and cathode voltage drops obtained in experiments I and II for the small and large electrodes at a temperature of 1615°K are shown in Fig. 3. For the identical upstream wall case of experiment I, small-electrode drops at a given current were found to be greater than corresponding large-electrode drops at both the anode and cathode. This indicates superior performance of the larger electrode for a fixed boundary-layer conductivity. This is reflected too by the slope of the voltage drop curves $\Delta V/\Delta I$, which is a measure of the electrode boundary-layer resistance. Except for cathodes at currents greater than about 4 amp (where arcing was believed to be prominent), the local resistance at the large electrode is less than that at the small electrode throughout experiment I. At anodes, the boundary-layer resistance for a given electrode size is constant over most of the current range. The tendency at the small electrode toward a decreasing resistance at high currents is attributed to non-negligible joule heating of the electrode boundary layer.

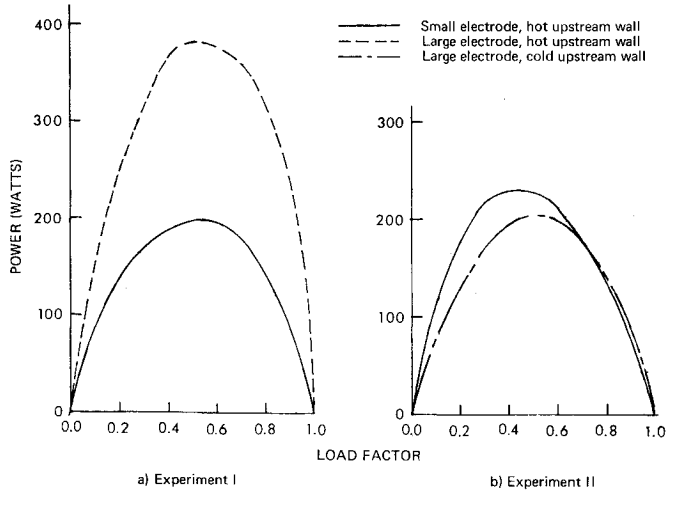

Fig. 4 Power characteristic curves for a single electrode pair of a given size (anode-cathode composites), $T_{\text{electrode}}$ = 1615°K.

The effects of a change in boundary-layer temperature on the performance of the large electrode can be seen by comparing, in Fig. 3, the results of the first and second experiments. Both anode and cathode voltage drops have increased substantially at the large electrode, while small electrode drops are reproduced to within 10 v of their previous values at all levels of current. Again, anode resistances for both electrode sizes are reasonably constant, decreasing slightly at higher currents. Cathode resistance decreases dramatically at the small electrode but only slightly at the large. The small electrode still suffers somewhat greater anode losses than the large electrode, but its cathode drops are far smaller than those at the large cathode.

In terms of total performance, the small electrodes now behave as well as large electrodes near open circuit, and slightly more favorably toward short circuit. This is more readily seen from the power characteristic curves of Fig. 4, which were obtained by forming, for each electrode size, a composite of the separate anode and cathode data. The power levels computed in each case include losses in the generator core, and employ the experimental values of open circuit voltage, which was about 170 v. These power levels will, of course, be different for geometries and operating conditions other than those used here.

Cold-Electrode Performance

At an electrode temperature of 530°K, voltage drop data from experiment I again showed that losses at the small electrode were greater than those at the large electrode, so that a larger electrode continued to give better performance for the same gas boundary-layer conditions. Cold-electrode results of experiment II with dissimilar upstream walls, however, showed voltage drops at the large electrode to be comparable to or greater than small electrode losses at both anode and cathode (Fig. 5). Thus, simulation of a cold-electrode generator for two electrode sizes demonstrated that coupling between electrode and boundary-layer temperatures may, in fact, lead to a reversing of preferable electrode size relative to the case of a hot-electrode generator, as indicated by the composite power characteristic curves of Fig. 6. These curves compare data for the simulated cold-electrode generator to those of the simulated hot-electrode generator shown earlier.

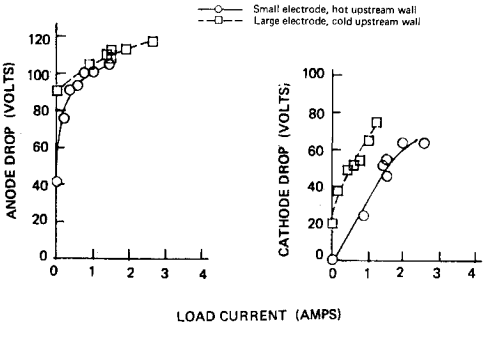

Fig. 5 Electrode voltage drop vs current, dissimilar upstream walls (experiment II), $T_{\text{electrode}}$ = 530°K.

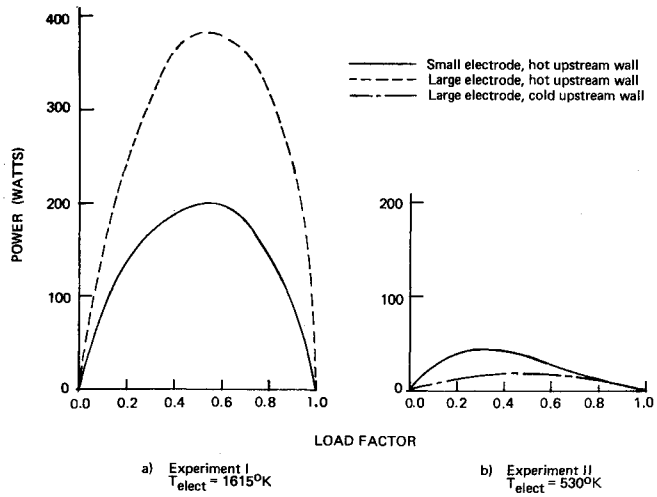

Fig. 6 Power characteristic curves for a single electrode pair of a given size (anode-cathode composites).

Again it is pointed out that the curves pertain to the geometry of the Stanford MHD channel.

In addition to an effect of electrode size, Fig. 6 also reveals a significant degradation in total power output for 530°K electrodes relative to 1615°K electrodes. This was caused by increases in both cathode and anode voltage drops. It was the change in anode drops, however, which were—both qualitatively and quantitatively—most severe. Such behavior was not anticipated from the findings of Kessler and Eustis,[2] whose experiments showed anode drops to reflect an essentially gasdynamic loss mechanism for electrode temperatures as low as 775°K. In experiment III, then, the range of electrode temperatures between 500°K and 1000°K was more carefully investigated using the small and medium electrode sizes. The electrode voltage drops obtained at the lower of the two total mass flow rates employed are shown in Fig. 7. From these data, an approximate boundary-layer resistance taken as the slope $\Delta V/\Delta I$ near open circuit was evaluated. Figure 8 shows such resistances displayed as a function of electrode temperature for anodes and cathodes at two mass flow rates. The sudden increase in anode resistance seen at electrode temperatures below about 700°–800°K agrees well with the hypothesis that large anode drops at and near open circuit were caused by deposition on the electrode surface of a solid, electrically resistive material, possibly one of several potassium-oxygen compounds whose melting points lie between 630° and 760°K.[14]

A model of cold-electrode performance was postulated to include an electrical resistance due to such a deposit in addition to the resistance associated with the gasdynamic boundary layer. (The latter is dependent on electrode size in that current flowing uniformly through the gas core must constrict to the electrode area at the wall.) The resistance of a solid deposit was estimated, and found to be larger than the gasdynamic resistance by more than an order of magnitude. Thus, anode voltage drops at low currents would likely be controlled by the resistivity and thickness of the electrode deposit, and the expected anode drops would be similar to those observed experimentally. For somewhat higher currents, at an anode voltage drop of about 80 v in the present experiments, arc spots were observed at the anode surface. It is believed that these arcs carry through the poorly conducting solid deposit so that the deposit then has only a minor influence on electrode performance. An electrode size effect due to current constriction remains, however. At a cold cathode, on the other hand, it is believed that small arcs are established nearly immediately to provide electron emission, since, even in the absence of an electrode deposit, currents attributable solely to uniform thermionic emission are virtually negligible. Thus, the electrode deposit, in the presence of

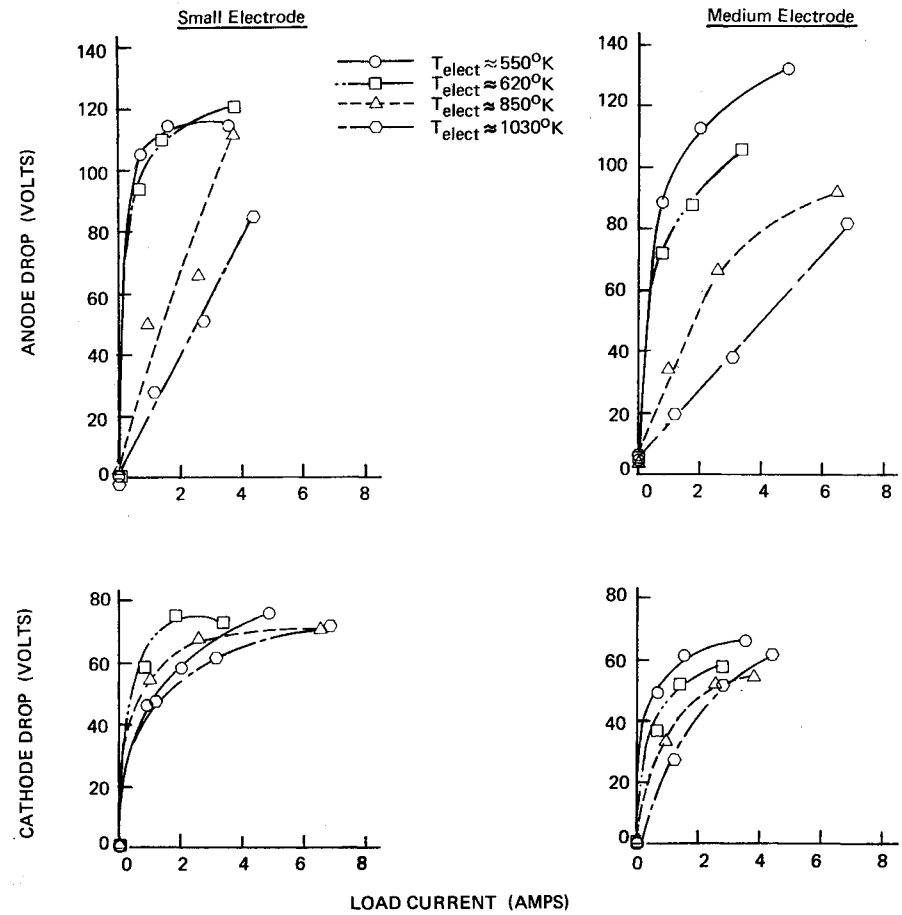

Fig. 7 Electrode voltage drop vs current, identical upstream walls (experiment III), $\dot{m}$ = 0.11 kg/sec.

these arcs, has little effect on cathode performance. Again, however, a gasdynamic size effect persists.

Attempts to interpret cold anode data in terms of other mechanisms such as gasdynamic effects, electron attachment, and low-temperature chemical reactions between the combustion gas and electrode coating proved unsatisfactory.[13] The curves of Fig. 8 thus indicate that the power levels shown in Fig. 6b would have been increased substantially were the electrode temperature about 200°K higher. The relative performance of small and large electrodes, however, would not be expected to change.

In general, motion pictures obtained with cold electrodes in all experiments revealed the presence of arc spots, on both anodes and cathodes, at all current densities above about 0.2 amp/cm^2. At lower currents no spots were visible, though arc activity of a low intensity could easily have gone undetected. The electrode perimeter was the generally preferred location for arc spots, with cathode spots tending to appear at the downstream electrode edge and anode spots at the upstream edge.

V. Interpretation of Results

Electrical Model of the Boundary Layer

Electrical results are interpreted in terms of a model proposed by Kessler and Eustis[2] in which the total resistance of an electrode boundary layer is assumed to be distributed among the gasdynamic boundary layer, the electrode surface, and the electrode sheath, which is the interface between the surface and the gasdynamic boundary layer. Resistance of the gasdynamic layer is considered to be purely ohmic, and is fixed by the geometry and the gas conductivity profile. Surface and sheath resistances, however, may be nonconstant and are typically associated with electron emission from cold electrodes. The extent of the sheath region from the surface is taken to be one Debye length which is the approximate distance over which departure from charge neutrality may exist.

Since the separate contributions of surface and sheath resistances are difficult to assess theoretically, the present analysis considers the two together as distinguished from the gasdynamic resistance, which is better understood, and for which quantitative analytical models exist. Differences between experimental voltage drops and calculated gasdynamic drops then give a measure of the combined surface-sheath losses.

Gasdynamic resistance was calculated using two analytical models. The first is an approximate model in which current flow is assumed to be uniformly distributed in the axial direction. The gasdynamic boundary-layer resistance, R_{BL}, corresponding to the rate of change of electrode voltage drop with load current is then given by

$$R_{BL} = \frac{1 + \bar{\beta}^2}{A_{\text{electrode}}} \int_{\lambda_D}^{\delta} \frac{dy}{\sigma(y)} - \frac{\delta}{\sigma_c A_c} \qquad (1)$$

where δ is the boundary-layer thickness, λ_D is the local Debye length, A is a cross-sectional area for uniform current conduction, σ is the scalar electrical conductivity, and $\bar{\beta}$ is the mean Hall parameter in the boundary layer. The subscript c denotes the gas core, where conditions are constant and where the electrical conductivity may be closely approximated by its scalar value.[13] Following Ref. 2, Eq. (1) assumes that the boundary-layer conduction area is equal to the electrode area, and that the tensor conductivity σ_β is given by

$$\sigma_\beta(y) = \sigma(y)/(1 + \bar{\beta}^2) \qquad (2)$$

The boundary-layer thickness δ is determined from the equation[10]

$$\delta = 0.32\ (x)(Re_x^{-0.2}) \qquad (3)$$

where Re_x is the length Reynolds number at a distance x from the channel inlet. Determination of the gasdynamic resistance is thus reduced to an integration of the conductivity profile through the boundary layer. For a fixed conductivity profile, resistance varies inversely with electrode size.

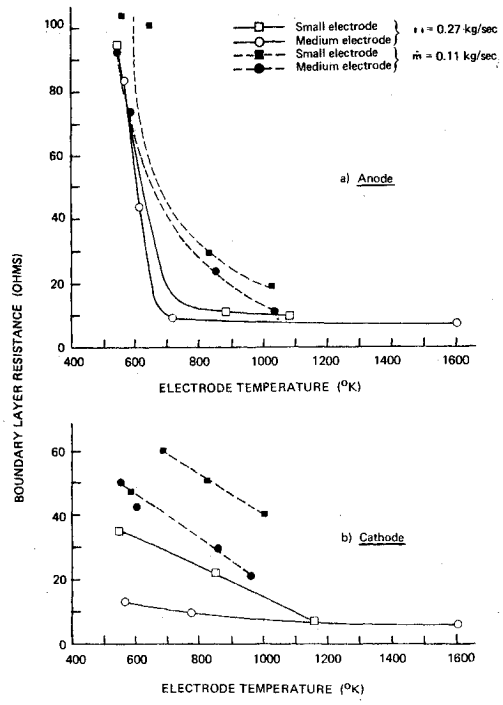

Fig. 8 Approximate boundary-layer resistance vs electrode temperature for a hot upstream wall (experiment III).

The second, more exact gasdynamic model considered, employs a numerical solution to Maxwell's equations and Ohm's law for a periodic channel geometry with finite electrode segmentation, and nonuniform electrical conductivity in the boundary-layer regions. The earlier assumptions concerning the direction and axial uniformity of the current flow are thereby relaxed, although the assumption of a diffuse current remains implicit.

Following the formulation of Oliver and Mitchner,[15] the equation

$$\partial^2\psi/\partial x^2 + \partial^2\psi/\partial y^2 - (\beta\partial \ln\sigma/\partial y)\partial\psi/\partial x - (\partial \ln\sigma/\partial y)\partial\psi/\partial y = 0 \qquad (4)$$

for the current stream function $\psi(x,y)$ is solved for model profiles of electrical conductivity using finite differences. The electrode-wall boundary conditions impose constant potential on electrodes, and zero normal current on insulators. The potential distribution is found from the current distribution by a numerical integration of Ohm's law. Electrode voltage drops are then determined, as in the experiments, by extrapolating the core potential profile to the electrode walls, and from this a boundary-layer resistance is determined. The boundary-layer thickness δ used in the computations is again obtained from Eq. (3), and the Hall parameter is obtained from Table 1.

In the gasdynamic region, the electrical conductivity profile was obtained from the boundary-layer enthalpy profile which spectroscopic measurements[13] had indicated was given by

$$[h(y) - h_w]/(h_c - h_w) = (y/\delta)^{1/7} \qquad (5)$$

Here, h is the static enthalpy, and the subscripts w and c refer to wall and gas core values, respectively. To obtain $\sigma(y)$, tabulated gas properties were used to relate enthalpy to temperature, then temperature to an equilibrium conductivity. The assumption of an equilibrium boundary layer was supported by auxiliary experiments specifically designed to

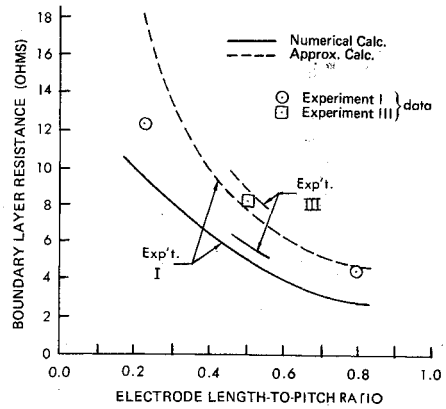

Fig. 9 Boundary-layer resistance vs electrode size: comparison of theoretical and experimental results for a hot anode and a hot upstream wall.

elucidate the presence of any significant nonequilibrium effects under conditions of the present experiments. No such effects could be discerned, so that nonequilibrium considerations were believed to be negligible in the present analysis.

For the isothermal wall condition approximated by hot electrodes and a hot upstream wall, Eq. (5) was taken as valid throughout the gasdynamic region, and wall enthalpy was evaluated at the electrode temperature. For cases of larger temperature differences between electrodes and the upstream wall, Eq. (5) was assumed to apply only at the upstream wall temperature, and the near-wall enthalpy profile was modified using the results of Refs. 16 and 17 for velocity and temperature steps in air. These results were found to adequately describe the data of previous MHD experiments.[2]

Equation (5) formed the basis for the conductivity profile used in the approximate gasdynamic model. In the "exact" numerical model, an analytical expression of the form

$$\frac{\sigma(y)}{\sigma_e} = \begin{cases} (y/\delta)^{\alpha} + \log_{10}\gamma, & y > 0,\ \sigma/\sigma_e < 1 \\ 1, & y > 0,\ \sigma/\sigma_e < 1 \\ \sigma_w, & y = 0 \end{cases} \qquad (6)$$

was used to approximate the "true" profile obtained using Eq. (5). The constants α and γ were determined graphically to best fit the curves in the spatially resolvable region of the computer program ($y/\delta > 0.03$), while the conductivity at one Debye length σ_w was assigned at the electrode wall. In the core of the channel the dimensionless conductivity was constant and equal to unity.

Discussion of Experimental Results

The effect of electrode size on generator performance for a fixed conductivity profile is indicated by the data of experiments I and III at an electrode temperature of 1600°K. The resistances determined from the slope of the anode drop curves for three electrode sizes at that temperature are shown in Fig. 9. The data are compared to the theoretical variations of resistance predicted by both the approximate and more exact gasdynamic models. For both experiments the boundary-layer thickness δ was found to be 13 mm, and the Debye length λ_D was 2×10^{-4} cm. Some comparisons of experimental and calculated resistances at the lower mass flow and at other electrode and boundary layer temperatures are given in Table 2.

The variation of anode boundary-layer resistance with electrode size is seen in Fig. 9 to be well described by the gasdynamic models. The two-dimensional numerical solution most closely predicts the relative performance of the three electrode sizes, though quantitative values are slightly low. This may be attributed to small systematic uncertainties in the near-wall conductivity profile, and in the Hall parameter and gas boundary-layer thickness. The approximate solution also gives good results for the larger electrode sizes, but becomes poorer for small electrodes because of the assumptions of a constant conduction area (the electrode value) and a constant direction of current flow (mean Hall angle). In general, however, Fig. 9 and Table 2 indicate that the effects of electrode size and temperature on the performance of anodes can be attributed to gasdynamic effects, except for the case of low electrode temperatures where condensation and solidification was believed to occur.

Gasdynamic effects were also found to govern cathode behavior for the case of the hottest (1600°K) electrodes with a hot upstream wall, for current densities not exceeding those of uniform thermionic emission, or about 1.0 amp/cm² (Ref. 18). In such cases the boundary-layer resistances indicated by the cathode drop characteristics were very nearly constant and were equal to the corresponding anode resistances for a given electrode size.

For cathode operation at current densities above saturated thermionic emission (at both high and low electrode temperatures), surface-sheath effects appeared to become prominent. At low currents, the effect was manifested by an increase in electrode voltage drop over that expected solely from gasdynamic considerations. This increase is believed to reflect the expenditure of energy required to draw electrons from a cold cathode surface. At high currents, the cathode voltage drop remained nearly constant. This mode of operation is thought to be associated with the formation of constricted arcs, in which energy is dissipated in joule heating of the gas and in heating of the electrode surface.

VI. Conclusions

The following conclusions may be drawn from this work:

1) For the segmented-Faraday mode of a combustion-driven MHD generator, an influence of electrode size on generator performance exists which is manifested by lower voltage losses at a larger electrode for similar conditions of surface and gas boundary-layer temperature.

2) Decreasing electrode temperature worsens electrode performance, but a larger electrode size continues to have lower losses for a given temperature of the gas boundary layer.

3) For dissimilar boundary-layer temperatures, a marked change may occur in the relative performance of different electrode sizes at the same surface temperature. In the present experiments, simulation of the coupling which may exist between electrode and boundary-layer temperatures in a cold-electrode generator yielded voltage losses which were greater for a large electrode with a cold upstream wall than for a small electrode with a hot upstream wall.

4) Voltage losses at a sufficiently hot anode reflect an essentially gasdynamic dependence on electrode size and temperature, and are reasonably well predicted by a two-dimensional analytical model incorporating a variable electrical conductivity in the boundary layers.

Table 2 Comparisons of theoretical and experimental anode resistance for several cases

Case						
Exp.	Flow, kg/sec	Size	T_{elect}	Approx calc.	Num. calc.	Exp.
I	0.27	sm	1615°K	18Ω	9Ω	12Ω
		lg	1615	4	3	4
II	0.27	lg	1615	7	8	9
III	0.27	sm	890	17	8	11
		med	1600	9	6	8
	0.11	sm	1030	29	12	19
		med	850	17	12	24

5) In most instances, cathode drops typically reflect surface-sheath losses in addition to gasdynamic losses. These losses decrease with increasing electrode temperature and vary nonlinearly with current.

6) Operation of electrodes below about 700–800°K in potassium seeded combustion gases causes large increases in anode voltage drops. This is believed due to deposition of a resistive solid deposit on the electrode surface.

References

[1] Sutton, G. W. and Sherman, A., *Engineering Magnetohydrodynamics*, McGraw-Hill, New York, 1965, pp. 478–480.

[2] Kessler, R. and Eustis, R. H., "Effects of Electrode and Boundary-Layer Temperature on MHD Generator Performance," *AIAA Journal*, Vol. 6, No. 9, Sept. 1968, pp. 1640–1646.

[3] Hurwitz, H., Jr., Kilb, R. W., and Sutton, G. W., "Influence of Tensor Conductivity on Current Distribution in an MHD Generator," *Journal of Applied Physics*, Vol. 32, No. 2, Feb. 1961, pp. 205–216.

[4] Witalis, E. A., "Analysis of Linear MHD Power Generators," *Journal of Nuclear Energy: Part C; Plasma Physics*, Vol. 7, 1965, pp. 455–473.

[5] Celinsky, Z. N. and Fischer, F. W., "Effects of Electrode Sizes in MHD Generators with Segmented Electrodes," *AIAA Journal*, Vol. 4, No. 3, March 1966, pp. 421–428.

[6] MacDonald, J. R., Mitchner, M., and Oliver, D. A., "Electrode Size Effects in an MHD Generator with Nonuniform Electrical Conduction," *AIAA Journal*, Vol. 5, No. 5, May 1968, pp. 948–949.

[7] Mori, F., Fushima, K., and Ikeda, S., "Experiments on MHD Power Generation with ETL Mark II," *Electricity from MHD, 1968*, Vol. 4, IAEA, Vienna, 1968, pp. 2761–2768.

[8] Louis J. F., Gal, G., and Blackburn, P. R., "Detailed Theoretical and Experimental Study on a Large MHD Generator," *AIAA Journal*, Vol. 3, No. 8, Aug. 1965, pp. 1487–1490.

[9] de Montardy, A. and Pericart, J., "Electrical Performance of a Duct with Segmented Electrodes under Various Conditions," *AIAA Journal*, Vol. 6, No. 9, Sept. 1968, pp. 1633–1639.

[10] Reseck, K. G., "Performance Characteristics of a Combustion-Driven Magnetogasdynamic Power Generator," SU-IPR 87, Aug. 1966, Institute for Plasma Research, Stanford Univ., Stanford, Calif.

[11] Kessler, R., "Effects of Electrode Temperature on MHD Generator Performance," SU-IPR 239, June 1968, Institute for Plasma Research, Stanford Univ., Stanford, Calif.

[12] Podolsky, B. and Sherman, A., "Influence of Tensor Conductivity on End Currents in Crossed Field MHD Channels with Skewed Electrodes," *Journal of Applied Physics*, Vol. 33, No. 4, April 1962, pp. 1414–1418.

[13] Rubin, E. S., "Effects of Electrode Size on the Performance of a Combustion-Driven MHD Generator," SU-IPR 335, Aug. 1969, Institute for Plasma Research, Stanford Univ., Stanford, Calif.

[14] Weast, R. C., ed., *Handbook of Chemistry and Physics*, 50th ed., The Chemical Rubber Co., Ohio, 1969, pp. B-143, B-145.

[15] Oliver, D. A. and Mitchner, M., "Nonuniform Electrical Conduction in MHD Channels," *AIAA Journal*, Vol. 5, No. 8, Aug. 1967, pp. 1424–1432.

[16] Simpson, R., Kays, W. M., and Moffat, R. J., "The Turbulent Boundary Layer on a Porous Plate: An Experimental Study of the Fluid Dynamics with Injection and Suction," HMT-2, Dec. 1967, Thermoscience Div., Mechanical Engineering Dept., Stanford Univ., Stanford, Calif., pp. 88–90.

[17] Reynolds, W. C., Kays, W. M., and Kline, S. J., "Heat Transfer in the Turbulent Incompressible Boundary Layer. II-Step Wall-Temperature Distribution," Memo 12-2-58W, 1958, NASA.

[18] Biblarz, O., "Discharge Characteristics in a Seeded, Flowing Plasma," Ph.D. thesis, 1968, Dept. of Mechanical Engineering, Stanford Univ. Stanford, Calif.